Photocatalytic Activities of Rutile and Anatase Nanoparticles Selectively Prepared from an Aqueous Solution

Munehiro SAKANOUE, Yasuhiro KINOSHITA, Yuichi OTSUKA and Hiroaki IMAI

Department of Applied Chemistry, Faculty of Science and Technology, Keio University, Hiyoshi, Kohoku-ku, Yokohama   223–8522

Nanoscale particles of rutile- and anatase-type titanium dioxides were selectively grown in acidic solutions of titanyl sulfate. The variation of photocatalytic activity as a function of UV light intensity was investigated using rutile and anatase powders having almost the same size (20–30 nm) and shape for a clear comparison of the performance depending on the crystal structure. Whereas the performance of anatase evaluated with the decomposition of methylene blue and the reduction of Cr(VI) under UV light was proportional to the square root of the UV light intensity, rutile showed a saturation of the activity in the high-intensity region regardless of the light sources and photochemical reactions. The saturating tendency of rutile weakened with an electron-withdrawing reaction or a decrease in the grain size. Then, the performance of rutile could be superior to that of anatase under illumination at a low-light-intensity. The difference in the photocatalytic performance between rutile and anatase is tentatively ascribed to a high recombination rate of generated electrons and holes associated with a low mobility of carriers in rutile.   [Received August 30, 2007; Accepted September 20, 2007]

Key-words : TiO₂, Photocatalysis, Titania, Polymorph, Nanoparticle, Optical property

1. Introduction

Titanium dioxide (TiO$_2$) photocatalysts have attracted much attention in diverse applications since the discovery of the photochemical dissociation of water on an oxide surface.[1] The photocatalytic activity of TiO$_2$ consisting of a rutile and/or anatase structure was studied,[2]–[8] and it is generally concluded that the photocatalytic activity of anatase is higher than that of rutile. Although the essence of the difference has not been sufficiently clarified, the lower energy level for the bottom of the conduction band or the higher recombination velocity of electron-hole pairs appears to be one of the reasons for the lower activity of the rutile structure.[9] The surface properties were also found to influence the different behaviors of rutile and anatase.[10],[11] Moreover, the electrical conductivity and charge carrier dynamics for the TiO$_2$ crystals were investigated by means of various techniques.[12]–[16] The difficulty in comparing the activities of both the crystal structures was the difference in the powder property and the surface condition originating from the preparation routes and resources. Usually, it is hard to prepare fine particles of rutile using conventional methods, while nanoscale anatase crystals are easily obtained by vapor- and aqueous-phase routes.[17] Recently, the superiority of rutile having a high specific surface area prepared through a solution route was reported.[18] However, a new technique to prepare anatase and rutile powders with the same size, shape, and crystallinity using the same raw material is desirable so that comparisons of photocatalytic activities according to their crystal structures can be made.

In our previous work, crystalline TiO$_2$ powders having almost the same size and shape were prepared by a direct deposition method in titanyl sulfate (TiOSO$_4$) solutions.[19]–[21] A crystal structure, such as rutile or anatase, was controlled by varying the pH, the concentration of TiOSO$_4$, or the amount of urea without changing the powder property. The specific surface area depending on the grain size was varied with post-annealing at various temperatures. Here, we successfully compared the photocatalytic activities of both the crystal structures using the powdery samples prepared with this technique. A difference in activity between anatase and rutile was found on the basis of the dependence of the performance on UV light intensity. Consequently, we observed saturation of the photocatalytic performance on rutile powder in a high-intensity region, whereas the activity of anatase increased in proportion to the square root of the intensity. Clarification of the saturation of the performance is important in order to understand the effects of photochemistry on oxide semiconductors and to develop phtocatalytic applications.

2. Experimental procedure

Precursor solutions at a titanium concentration of 0.01 M (mol dm^{-3}) were prepared by dissolving titanyl sulfate hydrate (TiOSO$_4 \cdot x$H$_2$O, $x = 4.6$, Nacalai Tesque) into purified water containing hydrochloric acid at pH 0.6 and 1.0 for preparation of rutile and anatase, respectively.[19]–[21] A specific amount of urea ((NH$_2$)$_2$CO, Junsei Chemical) ([(NH$_2$)$_2$CO]/[TiOSO$_4$] = 150) was added to promote the formation of highly crystalline anatase through control of the precipitation rate with complexation and a gradual increase in pH with decomposition.[21] After the solutions contained in a polypropylene vessel were kept at 60°C for 24 h in an electric oven, precipitation of crystalline TiO$_2$ occurred. High-purity cotton fibers were used as a substrate for deposition of TiO$_2$ crystals for promotion of nucleation and subsequent crystal growth. The deposited crystals were dried at 60°C for 24 h in air, and then calcined at 500°C for 3 h in air. The heating process was required for the removal of strongly attached water and residual urea affecting the photocatalytic activity from the surface and interface of the crystal grains. The cotton substrate was completely removed through combustion at 500°C for 3 h in air. Rutile powder having a high specific surface area of ca. 200 m^2/g was prepared with calcination of the precipitates at 300°C for 3 h in air to investigate the influence of the surface area on the saturation tendency. In this case, the removal of cotton with calcinations at a higher temperature was not necessary because the powder deposited on the bottom and the wall of the plastic vessels was utilized for the evaluation.

Characterization of the TiO$_2$ powders was performed by X-ray diffractometry (XRD) with a Rigaku RAD–C system and Fourier-transform infrared (FTIR) spectrometry with a BIO–RAD FTS–65. Scanning electron micrographs (SEM) and transmission electron micrographs (TEM) were obtained using a Hitachi S–4700 and Philips TECNAI F20, respective-
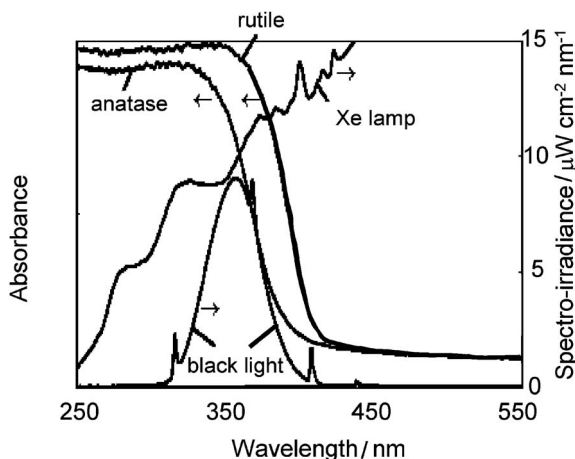
Fig. 1.   Absorption spectra of rutile and anatase powders prepared in solutions and spectral distribution of a black light and a Xe lamp.

rutile
(s.s.a. 50.5 m^{2}g^{-1})   anatase
(s.s.a. 47.0 m^{2}g^{-1})

Fig. 2.   Electron micrographs of rutile and anatase powders calcined at 500°C. SEM images of rutile (a) and anatase (b), and TEM images of rutile (c) and anatase (d). These powders had almost the same specific surface area (s. s. a).

ly. Nitrogen absorption isotherms were recorded using a Micromeritics TriStar 3000. Diffuse reflectance spectroscopy (DRS) in a UV-vis region was carried out with a JASCO V-550.

The photocatalytic activity was evaluated by the decomposition of methylene blue (MB) in water under UV from a conventional black light (6 W × 2) or a solar simulator using a xenon (Xe) lamp (500 W). Spectral distribution of the light sources is shown in **Fig. 1**. The decomposition of MB in water under illumination was measured with 0.25 g powders deposited on the bottom of an open container of 60 cm^3 in volume. A powder bed with an area of 27 cm^2 was prepared through drying of a suspension of the sample powder in the container. Then, a solution of 30 cm^3 containing 20 ppm MB was gently poured on the powder bed. The UV light was irradiated on the powder bed through the solution of 1.1 cm in thickness. The solution was frequently stirred during the illumination. The pH of the solution (ca. 5) was not changed by the contact with the sample powders and by the illumination. The direct decomposition of MB was negligible under the illumination. The reduction of Cr (VI) into Cr (III) was performed with 0.04 g of powder dispersed in a glass vessel containing a 500 μM solution of K$_2$Cr$_2$O$_7$. Nitrogen gas was introduced with a flow rate of 100 cm^3 min^{-1} into the solution adjusted to pH 2 with sulfuric acid under UV illumination from a black light. The irradiated area for the chromium solution was 16 cm^2. The variation of the concentrations of MB and Cr$_2$O$_7^{2-}$ was monitored with the specific absorption bands at 665 and 352 nm, respectively, using a Shimadzu UV2500 UV-vis spectrometer. The dependence on the intensity of illumination was investigated with variation of the distance between the sample vessel and the light source. The intensity of UV light at the sample powder was estimated by a Shiro SUV-340 UV sensor, which was sensitive to photons in the range of 290–390 nm in wavelength. Almost all the photons illuminated from a black light and more than 80% of UV photons from a Xe lamp were covered by this detector.

3.   Results and discussion

Fine particles of crystalline TiO$_2$ were directly produced through deposition in aqueous solutions at 60°C. The polymorphs grown in the precursor solutions were predominantly controlled by the initial pH. Pure rutile and anatase were selectively produced in the solutions at pH 0.6 and 1.0, respec-
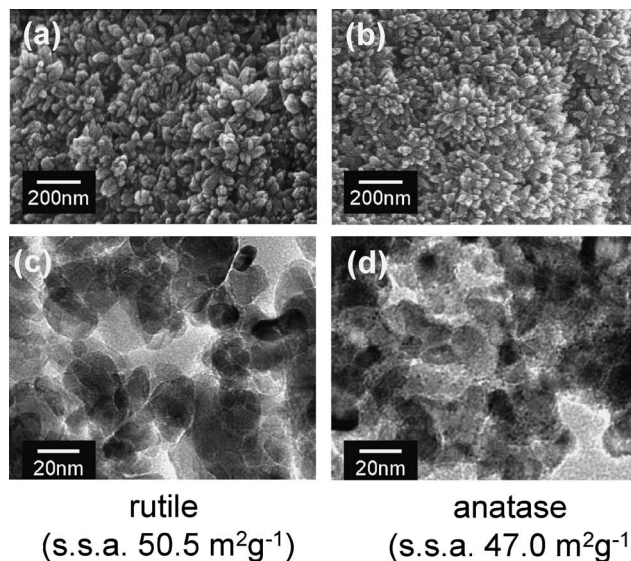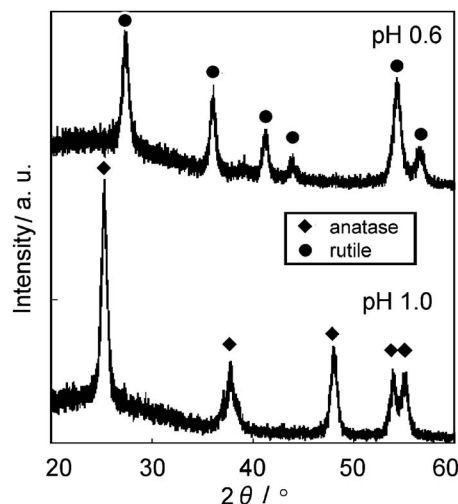

Fig. 3.   XRD patterns of powders prepared in TiOSO$_4$ solutions at pH 0.6 and 1.0, respectively, and then calcined at 500°C.

tively. As-deposited crystals were obtained as a bundle of needles ca. 5 nm in diameter. They exhibited a high specific surface area of about 200 m^2 g^{-1} regardless of the crystal structure.[21] However, calcination at 500°C in air was required for a decrease in the amount of surface impurities, such as strongly attached water and the remaining sulfate and urea, to eliminate materially the influence of the surface property on the photocatalytic activity. The heating process increased the grain size to 20–30 nm through sintering of the needles in the bundles as shown in SEM and TEM images (**Fig. 2**), whereas the crystal structures were not changed as shown in XRD patterns (**Fig. 3**). Consequently, using Scherrer's equation, the crystallite sizes for calcined rutile and anatase were estimated to be almost the same (ca. 28 nm) along the c axis from the X-ray diffraction peaks. The similarity of the grain sizes was supported by the results of an evaluation of specific sur-
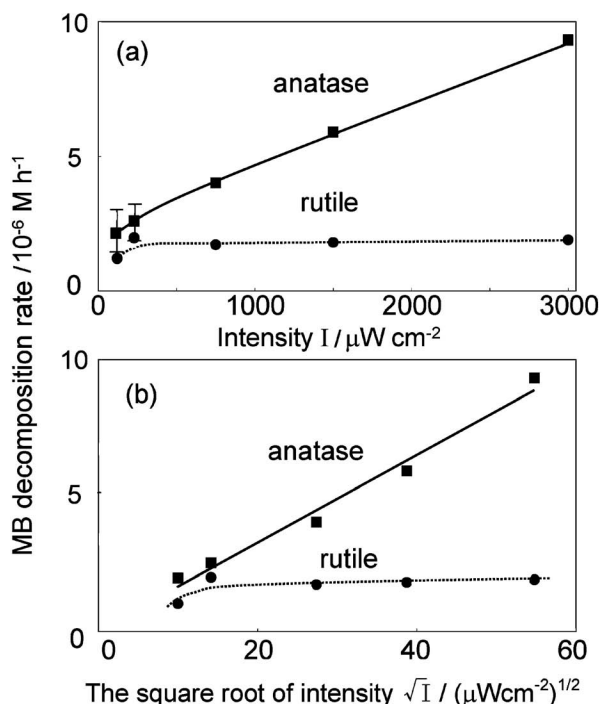
Fig. 4. Decomposition rate of MB as a function of the intensity of UV light (a) and the square root of the intensity (b) under irradiation from a Xe lamp.
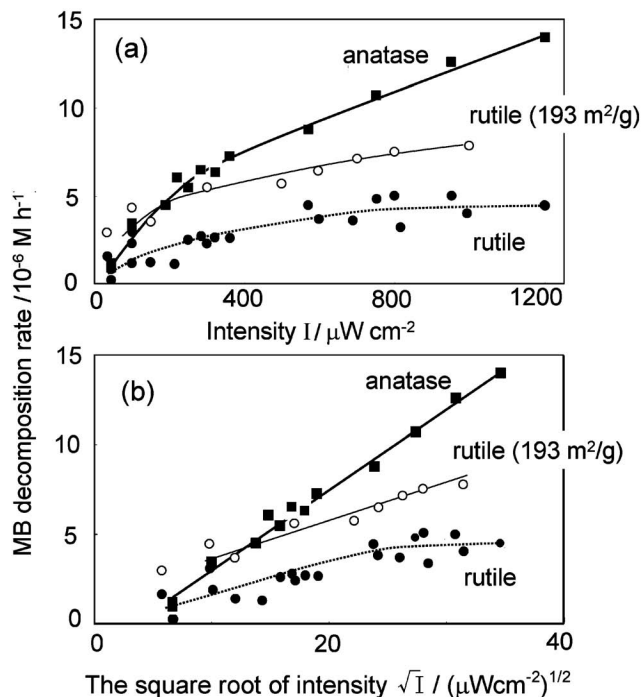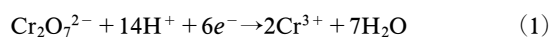

Fig. 5. Decomposition rate of MB as a function of the intensity (a) and the square root of the intensity (b) under UV irradiation from a black light.

face areas (s.s.a.) (ca. $50 \, m^2 \, g^{-1}$). Finally, using the same procedure and the same raw materials, we obtained pure rutile and anatase powders having almost the same size, which we used as standard samples to compare the photocatalytic activity. Because DRS in a UV-vis region (Fig. 1) showed no additional peaks around the absorption edge, oxygen deficiency was not induced during the preparation of the crystals and the subsequent procedure.

We mainly evaluated the dependence of photocatalytic activity using standard rutile and anatase powders on the UV light intensity from a solar simulator with a Xe lamp. The photocatalytic activity was estimated from the average decomposition rate of MB in the initial three hours. In this period, the concentration of MB decreased almost linearly under the illumination. As shown in **Fig. 4**, the performance of anatase monotonically increased as the intensity of the light was increased, and the decomposition rate was almost proportional to the square root of the intensity. On the other hand, the activity of rutile showed a steep saturation in a low-intensity region. The quantum yields of the decomposition (the ratio of the number of decomposed molecules to the number of absorbed photons) with rutile and anatase were almost the same at $100\text{–}200 \, \mu W \, cm^{-2}$, although that of anatase was five times larger than that of rutile at $3 \, mW \, cm^{-2}$. The low value of the quantum yield (ca. 0.2% at $100\text{–}200 \, \mu W \, cm^{-2}$) is attributable to involved, multistep procedures for the decomposition of MB molecules with photocatalysts.[22),23)]

Figure 5 shows the dependence of the photocatalytic activity of the standard rutile and anatase powders for the MB decomposition on the intensity of UV illumination from a black light. We also observed saturation of the activity for the decomposition of MB with rutile powder, whereas the decomposition rate with anatase was proportional to the square root of the intensity. Consequently, a difference

between rutile and anatase in the dependence on light intensity was observed regardless of the spectral distribution of the incident light. The photocatalytic activity of smaller rutile grains calcined at $300°C$ in air is also shown in Fig. 5. The saturating tendency was weakened and the performance was increased with the smaller grains ($< 10 \, nm$) of rutile having a high specific surface area ($193 \, m^2 \, g^{-1}$). On the other hand, the performance of smaller grains of anatase calcined at $300°C$ having a high specific surface area above $200 \, m^2 \, g^{-1}$ was similar to that of the standard anatase (not shown). Therefore, a decrease in the grain size was found to be effective in boosting the activity only for rutile. Moreover, the performance of fine particles of rutile could be superior to that of anatase in a low-intensity region.

Photocatalytic performance commonly depends on the sorts of chemical reaction. Thus, we evaluated the dependence of photocatalytic activity on UV intensity using the reduction of $Cr(VI)$ into $Cr(III)$ in a $Cr_2O_7^{2-}$ solution.[24)–26)] As shown in **Fig. 6**, saturation behavior and square-root dependence on the light intensity were observed with rutile and anatase, respectively. This fact suggests that the saturation of the activity of rutile is generally observed in a variety of photocatalytic reactions. In this case, however, the saturating tendency was observed in a relatively high-intensity region (ca. $5 \, mW \, cm^{-2}$) in comparison with the decomposition of MB. Moreover, the performance of the rutile was slightly superior to that of anatase in the low-intensity region. The quantum yield of a reduction of $Cr_2O_7^{2-}$ in which six electrons participate was estimated to be about 5% at $1 \, mW \, cm^{-2}$. A relatively high yield is basically ascribed to a simple route of the photocatalytic reaction with a relatively small ion as expressed by Eq. (1),

$$Cr_2O_7^{2-} + 14H^+ + 6e^- \rightarrow 2Cr^{3+} + 7H_2O \qquad (1)$$
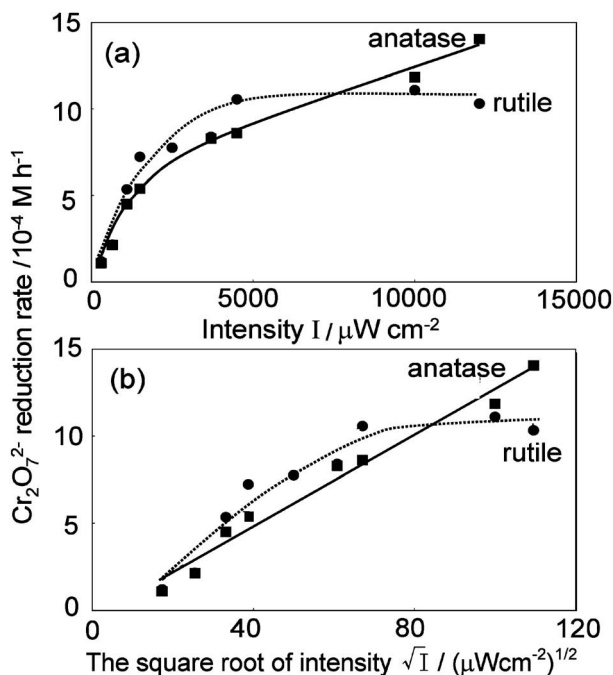
It is suggested that the UV-generated holes are trapped with

Fig. 6.   Reduction rate of $Cr_2O_7^{2-}$ as a function of the intensity (a) and the square root of the intensity (b) under UV irradiation from a black light.

water molecules.[26]

Previous studies[27)-29)] have reported that the quantum yield of photocatalytic reactions decreased as the light intensity increased. Thus, we generally observe the sublinear dependence of photocatalytic activity on light intensity. The decrease in the quantum yield can be ascribed to the recombination of generated electron-hole pairs or the deactivation of radical species through reactions with other species on the surface. Here, the photocatalytic activity of anatase was almost proportional to the square root of the UV intensity. According to previous reports,[28),29)] this phenomenon can be explained as follows. The reaction rates of photo-oxidation (R_{ox}) and reduction (R_{re}) were proportional to the density of photo-generated holes ($[h^+]$) and electrons ($[e^-]$), respectively,

$$R_{ox} = k_h[h^+][D_{ad}] \qquad (2\text{-}1)$$
$$R_{re} = k_e[e^-][A_{ad}] \qquad (2\text{-}2)$$

where $[D_{ad}]$ and $[A_{ad}]$ denote the density of adsorbed reactants for holes and electrons, respectively. Assuming the quantum yield is negligibly small in comparison to the recombination rate, the generation rate of electrons and holes, which is the product of the absorption coefficient (α) and the light intensity (I), is equal to the recombination rate, which is proportional to the product of the densities of electrons and holes at a steady state,

$$\alpha I = k_r[e^-][h^+] \qquad (3)$$

$$\alpha I = k_r \frac{R_{re}}{k_e[A_{ad}]} \frac{R_{ox}}{k_h[D_{ad}]} \qquad (3')$$

Because the reaction rates of photo-reduction and oxidation are apparently the same, the reaction rates should show a square-root dependence of the activity on the UV intensity,

$$R_{ox} = R_{re} = \left(\frac{k_e k_h}{k_r} [A_{ad}][D_{ad}] \right)^{1/2} \alpha^{1/2} I^{1/2} \qquad (4)$$

On the other hand, the photocatalytic activity of rutile showed a saturating tendency in a high-intensity region, whereas a square-root dependence of the activity was observed in a low-intensity region. The recombination rate of photo-generated electron-hole pairs in the rutile structure was deduced to be higher than that in the anatase.[9)] The effective mass of the charge carriers, such as generated electrons and holes in rutile is larger than those in anatase.[15)] Since electron-hole pairs generated in a deep region would be quenched through recombination before arriving at the surface due to their low mobility, rutile particles are presumed to have an inactive core surrounded by an active shell for the photocatalytic reaction. The thickness of the active shell is associated with the mean free path of the carriers, which is inversely proportional to the effective mass and the density of the carriers. This assumption leads to the conclusion that the thickness of the active shell of rutile is thinner than that of anatase and it decreases in inverse proportion to the square root of the UV intensity because the densities of generated electrons and holes are proportional to the square root of the intensity. The saturation of the activity of rutile is attributed to the balance between an increase in the densities of photo-generated electron-hole pairs and a decrease in the thickness of the active shell. In this case, the effective densities of holes and electrons for the photocatalytic reaction become constant independently of the UV intensity. On the other hand, the influence of the inactive core is negligible when the radius of the particles is smaller than the thickness of the active shell. Therefore, a decrease in grain size weakened the saturating tendency and then increased the activity of rutile powder in a high-intensity region. Saturation of the activity for the reduction of $Cr_2O_7^{2-}$ was observed at a higher intensity than that for the decomposition of MB. The weakening of the saturating tendency is also attributable to a decrease in the recombination probability caused by a rapid withdrawal of electrons from the TiO_2 particles through the reduction of $Cr_2O_7^{2-}$.

4. Conclusions

Pure rutile and anatase powders were selectively prepared through an aqueous solution route from the same starting materials. The dependence of photocatalytic activity on the crystal structure was clearly studied using the rutile and anatase powders that were nearly identical in size and shape. Saturation of the activity on the intensity of UV illumination was observed for rutile powder regardless of the light source and the chemical reaction. The characteristic behavior is ascribed to the quenching of photo-generated electron-hole pairs due to the low mobility of carriers in the rutile structure. A lower performance of rutile could be attributable to the saturating tendency of the activity when the light intensity was increased.

References
1) A. Fujishima and K. Honda, *Nature*, **238**, 37–38 (1972).
2) A. Sclafani, L. Palmisano and M. Schiavello, *J. Phys. Chem.*, **94**, 829–832 (1990).
3) M. Andersson, L. Österlund, S. Ljungström and A. Palmqvist, *J. Phys. Chem. B*, **106**, 10674–10679 (2002).
4) T. Sumita, T. Yamaki, S. Yamamoto and A. Miyashita, *Appl. Surf. Sci.*, **200**, 21–26 (2002).
5) T. Ohno, D. Haga, K. Fujihara, K. Kaizaki and M Matsumura, *J. Phys. Chem. B*, **101**, 6415–6419 (1997).
6) T. Ohno, K. Sarukawa and M. Matsumura, *J. Phys. Chem. B*, **105**, 2417–2420 (2001).
7) T. Ohno, K. Sarukawa and M. Matsumura, *New J. Chem.*, **26**, 1167–1170 (2002).

8) T. Ohno, K. Sarukawa, K. Tokieda and M. Matsumura, *J. Catal.*, **203**, 82–86 (2001).

9) K. Okamoto, Y. Yamamoto, H, Tanaka and A. Itaya, *Bull. Chem. Soc. Jpn.*, **58**, 2015–2022 (1985).

10) N. Spanos, I. Georgiadou and A. Lycourghiotis, *J. Collid Interface Sci.*, **172**, 374 (1995).

11) A. Sclafani and J. M. Herrmann, *J. Phys. Chem.*, **100**, 13655–13661 (1996).

12) Th. Dittrich, J. Weidmann, F. Koch, I. Uhlendorf and I. Lauermann, *Appl. Phys. Lett.*, **75**, 3980–3982 (1999).

13) A. Furube, T. Asahi, H. Masuhara, H. Yamashita and M. Anpo, *J. Phys. Chem. B*, **103**, 3120–3127 (1999).

14) V. Duzhko, V. Yu. Timoshenko, F. Koch and Th. Dittrich, *Phys. Rev. B*, **64**, 075204 (2001).

15) H. Tang, K. Prasad, R. Sanjinés, P. E. Schmid and F. Lévy, *J. Appl. Phys.*, **75**, 2042–2047 (1994).

16) H. Tang, K. Prasad, R. Sanjinés and F. Lévy, *Sensors and Actuators B*, **26–27**, 71–75 (1995).

17) I. N. Martyanov and K. J. Klabunde, *J. Catal.*, **225**, 408–416 (2004).

18) S.-J. Kim, J.-K. Lee, E.-G. Lee, H.-G. Lee, S.-J. Lim and K. S. Lee, *J. Mater. Res.*, **18**, 729–732 (2003).

19) S. Yamabi and H. Imai, *Chem. Mater.*, **14**, 609–614 (2002).

20) S. Yamabi and H. Imai, *Chem. Lett.*, **30**, 220–221 (2001).

21) S. Yamabi and H. Imai, *Thin Solid Films*, **434**, 86–93 (2003).

22) A. Houas, H. Lachheb, M. Ksibi, E. Elaloui, C. Guillard and J.-M. Herrmann, *Appl. Catal. B: Environ.*, **31**, 145–157 (2001).

23) T. Zhang, T. Oyama, S. Horikoshi, H. Hidaka, J. Zhao and N. Serpone, *Sol. Energy. Mater. Sol. Cells*, **73**, 287–303 (2002).

24) C. R Chenthamarakshan, K. Rajeshwar and E. J. Wolfrum, *Langmuir*, **16**, 2715–2721 (2000).

25) G. Colon, M. C. Hidalgo and J. A. Navio, *Langmuir*, **17**, 7174–7177 (2001).

26) L. A. García Rodenas, A. D. Weisz, G. E. Magaz and M. A. Blesa1, *J. Colloid Interface Sci.*, **230**, 181–185 (2000).

27) Y. Ohko, D. A. Tryk, K. Hashimoto and A. Fujishima, *J. Phys. Chem. B*, **102**, 2699–2704 (1998).

28) H. Al-Ekabi and P. DeMayo, *J. Phys. Chem.*, **89**, 5815–5821 (1985).

29) Y. Nosaka and M. A. Fox, *J. Phys. Chem.*, **92**, 1893–1897 (1988).